EUROPEAN ORGANIZATION FOR NUCLEAR RESEARCH (CERN)

CERN-EP-2022-108
LHCb-PAPER-2022-012
23 June 2023

# Study of exclusive photoproduction of charmonium in ultra-peripheral lead-lead collisions

LHCb collaboration[†]

**Abstract**

The cross-sections of exclusive (coherent) photoproduction $J/\psi$ and $\psi(2S)$ mesons in ultra-peripheral PbPb collisions at a nucleon-nucleon centre-of-mass energy of 5.02 TeV are measured using a data sample corresponding to an integrated luminosity of $228 \pm 10\,\mu\text{b}^{-1}$, collected by the LHCb experiment in 2018. The differential cross-sections are measured separately as a function of transverse momentum and rapidity in the nucleus-nucleus centre-of-mass frame for $J/\psi$ and $\psi(2S)$ mesons. The integrated cross-sections are measured to be $\sigma^{\text{coh}}_{J/\psi} = 5.965 \pm 0.059 \pm 0.232 \pm 0.262\,\text{mb}$ and $\sigma^{\text{coh}}_{\psi(2S)} = 0.923 \pm 0.086 \pm 0.028 \pm 0.040\,\text{mb}$, where the first listed uncertainty is statistical, the second systematic and the third due to the luminosity determination. The cross-section ratio is measured to be $\sigma^{\text{coh}}_{\psi(2S)}/\sigma^{\text{coh}}_{J/\psi} = 0.155 \pm 0.014 \pm 0.003$, where the first uncertainty is statistical and the second is systematic. These results are compatible with theoretical predictions.

Published in JHEP 06 (2023) 146



[†]Authors are listed at the end of this paper.

# 1 Introduction

Ultra-peripheral collisions (UPCs) occur when two nuclei collide with an impact parameter, the distance between their centres, larger than the sum of their radii [1]. Because the nuclei do not overlap, strong interactions are suppressed so that photon-induced interactions between the two ions dominate. The number of photons produced is proportional to the square of electric charge, so photon-nuclear interactions are significantly enhanced in lead-lead (PbPb) collisions compared to proton-proton ($pp$) collisions. In UPCs, $J/\psi$ and $\psi(2S)$ mesons can be produced from the colourless exchange of a photon from one of the two nuclei and a pomeron from the other. Coherent (exclusive) photoproduction occurs when the photon couples coherently with the entire nucleus through an exchange of a pomeron, while for incoherent photoproduction, the photon interacts with a particular nucleon within the nucleus. In this work, the terms "coherent" and "incoherent" charmonium photoproduction refer to the two diagrams, respectively, shown in Figure 1.

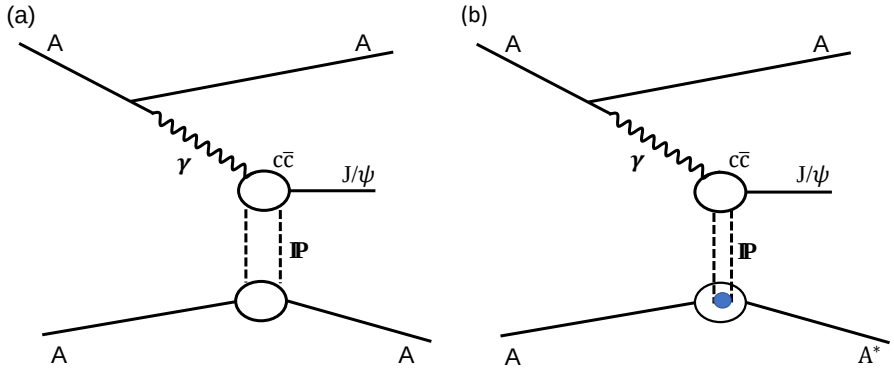


Figure 1: Schematic diagrams for charmonium production in (a) coherent and (b) incoherent UPC heavy-ion collisions. For incoherent production, the pomeron is emitted from a single nucleon, indicated by the blue dot, and the nucleus typically dissociates, indicated by $A^*$.

The coherent (exclusive) photoproduction of $J/\psi$ and $\psi(2S)$ mesons is expected to probe the nuclear gluon distribution functions at a momentum transfer of $Q^2 \approx m^2/4$, where $m$ is the mass of the meson. The photon-nuclear production of these mesons depends on the longitudinal momentum fraction of gluons in the nucleus, $x \approx (m/\sqrt{s_{\mathrm{NN}}})e^{\pm y}$, where $y$ is the rapidity of the meson and $\sqrt{s_{\mathrm{NN}}}$ is the nucleon-nucleon centre-of-mass energy. Thus, coherent photoproduction of charmonium mesons provides an excellent laboratory to study nuclear shadowing effects and the initial states of collisions with small $x$, where $10^{-5} \lesssim x \lesssim 10^{-2}$ at the LHC [2]. The charmonia produced in this process have typical transverse momenta, $p_{\mathrm{T}}$, smaller than 100 MeV/$c$, with no other particles produced in the collision. Coherent (exclusive) $J/\psi$ photoproduction was first measured in UPCs at HERA [3, 4] in electron-proton scattering, and with ions at RHIC [5]. This process has also been measured by the CMS experiment in the central region [6], by the LHCb experiment in the forward region [7], and by the ALICE collaboration in both the central and forward regions [8, 9] at $\sqrt{s_{\mathrm{NN}}} = 5.02$ TeV in PbPb collisions at the LHC.

This paper presents a measurement of the coherent $J/\psi$ and $\psi(2S)$ production reconstructed through the dimuon final state using the 2018 PbPb data sample collected by

the LHCb experiment at $\sqrt{s_{\rm NN}} = 5.02\,\text{TeV}$ and corresponding to an integrated luminosity of $228 \pm 10\,\mu\text{b}^{-1}$. The study also measures the ratio between the coherent $\psi(2S)$ and $J/\psi$ production cross-sections, where the uncertainties due to systematic effects and the luminosity determination largely cancel. This more precise measurement will help to constrain theoretical predictions, where uncertainties arise from the choice of the meson wave function in dipole scattering models [10,11] and the factorisation scale in perturbative QCD models [12].

The LHCb detector and simulation are described in Sec. 2. The selection of signal candidates and the determination of cross-sections are described in Sec. 3 and Sec. 4, respectively. The uncertainties due to systematic effects are described in Sec. 5, while the results are presented in Sec. 6 and conclusions are given in Sec. 7.

# 2 Detector, event reconstruction and simulation

The LHCb detector [13, 14] is a single-arm forward spectrometer covering the pseudorapidity range $2 < \eta < 5$, designed for the study of particles containing $b$ or $c$ quarks. The detector includes a high-precision tracking system consisting of a silicon-strip vertex detector surrounding the collision region, a large-area silicon-strip detector located upstream of a dipole magnet with a bending power of about 4 Tm, and three stations of silicon-strip detectors and straw drift tubes placed downstream of the magnet. The tracking system provides a measurement of the momentum, $p$, of charged particles with a relative uncertainty that varies from 0.5% at low momentum to 1.0% at 200 GeV/$c$. The minimum distance of a track to a primary $pp$ collision vertex, the impact parameter (IP), is measured with a resolution of $(15 + 29/p_{\rm T})\,\mu\text{m}$, where $p_{\rm T}$ is in GeV/$c$. Photons, electrons and hadrons are identified by a calorimeter system consisting of scintillating-pad (SPD) and preshower detectors, an electromagnetic and a hadronic calorimeter. Muons are reconstructed as a long track passing through the vertex detector and the three stations of silicon-strip tracking detectors, and identified by a system composed of alternating layers of iron and multiwire proportional chambers.

The pseudorapidity coverage is extended by forward shower counters (HeRSCheL) consisting of five planes of scintillators with three planes at 114, 19.7 and 7.5 m upstream of the LHCb detector, and two planes downstream at 20 and 114 m. The HeRSCheL detector [15] significantly extends the acceptance for detecting particles from dissociated nucleons by covering the pseudorapidity range of $5 \lesssim |\eta| \lesssim 10$, enhancing the classification of central exclusive production and UPC events.

The online event selection is performed by a trigger, which consists of a hardware stage, based on information from the calorimeter and muon systems, followed by a software stage, which applies a full event reconstruction.

Simulated events are used to determine corrections for the detector resolution, acceptance, and efficiency. The UPCs are modelled using STARlight [16] with a specific LHCb configuration [17]. The STARlight generator models coherent and incoherent vector-meson production in photon-nuclear interactions. Decays of unstable particles are described by EvtGen [18] with QED final-state radiation handled by Photos [19]. The interactions of the generated particles with the detector are modelled using the Geant4 toolkit [20, 21] as described in Ref. [22].

# 3 Selection of signal candidates

Signal candidates are reconstructed through the decays $J/\psi \to \mu^+\mu^-$ and $\psi(2S) \to \mu^+\mu^-$, and are required to have a rapidity within the range $2.0 < y^* < 4.5$, where the starred notation indicates that the observable is defined in the nucleus-nucleus centre-of-mass frame. All remaining selection criteria given here are defined in the laboratory frame. One of the candidate muons must pass the hardware-level trigger, which requires a muon $p_{\mathrm{T}}$ greater than 500 MeV/$c$. The dimuon candidates are selected with a minimum-bias software trigger, requiring at least one track reconstructed by the vertex detector; this software trigger is 100% efficient with respect to the following offline selection, since it has a looser multiplicity requirement. The offline selection requires two muon candidates, both with tracks that have $p_{\mathrm{T}} > 700\,\mathrm{MeV}/c$ within the pseudorapidity range $2.0 < \eta < 4.5$. The dimuon candidates are required to have $p_{\mathrm{T}} < 1\,\mathrm{GeV}/c$ and an azimuthal opening angle between the muons larger than $0.9\,\pi$. The mass of each signal candidate, $m_{\mu^+\mu^-}$, is required to be within $\pm 65\,\mathrm{MeV}/c^2$ of the known $J/\psi$ mass [23] or $\pm 77.35\,\mathrm{MeV}/c^2$ of the known $\psi(2S)$ mass [23]. To suppress background from PbPb collisions with impact parameter smaller than two times the nucleus radius, only events with less than 20 hits in the SPD are retained, corresponding to very low occupancy events that make up about 0.3% of all minimum-bias events. Additionally, a requirement based upon a figure of merit that combines the signals from all HeRSCheL stations [15], is used to discard events with significant activity in the HeRSCheL acceptance region.

# 4 Cross-section determination

For comparison with theoretical predictions, the measured cross-sections are transformed into the nucleus-nucleus centre-of-mass frame, from the laboratory frame, to account for the non-zero crossing angle between the two Pb beams. The differential cross-section for coherent charmonium production in a given interval of rapidity or transverse momentum is determined as

$$\frac{\mathrm{d}\sigma_{\psi}^{\mathrm{coh}}}{\mathrm{d}x} = \frac{N_{\psi}^{\mathrm{coh}}}{\mathcal{L} \times \varepsilon_{\mathrm{tot}} \times \mathcal{B}(\psi \to \mu^+\mu^-) \times \Delta x}\,, \tag{1}$$

where $\psi$ is either $J/\psi$ or $\psi(2S)$, $x$ represents either the $y^*$ or $p_{\mathrm{T}}^*$, $N_{\psi}^{\mathrm{coh}}$ is the coherent signal yield, $\varepsilon_{\mathrm{tot}}$ is the total efficiency, $\mathcal{L}$ is the integrated luminosity, $\Delta x$ is the width of either the $y^*$- or $p_{\mathrm{T}}^*$-interval, and $\mathcal{B}(\psi \to \mu^+\mu^-)$ is the branching fraction of the charmonium decay. The branching fractions $\mathcal{B}(J/\psi \to \mu^+\mu^-) = (5.961 \pm 0.033) \times 10^{-2}$ and $\mathcal{B}(\psi(2S) \to e^+e^-) = (7.93 \pm 0.17) \times 10^{-3}$ [23] are used. For the $\psi(2S)$ the more accurate dielectron branching fraction is used, where lepton universality is assumed. The ratio between the differential cross-sections of $\psi(2S)$ and $J/\psi$ production in a given rapidity interval is given by

$$\frac{\mathrm{d}\sigma_{\psi(2S)}^{\mathrm{coh}}/\mathrm{d}y^*}{\mathrm{d}\sigma_{J/\psi}^{\mathrm{coh}}/\mathrm{d}y^*} = \frac{N_{\psi(2S)}^{\mathrm{coh}} \times \varepsilon_{J/\psi} \times \mathcal{B}(J/\psi \to \mu^+\mu^-)}{N_{J/\psi}^{\mathrm{coh}} \times \varepsilon_{\psi(2S)} \times \mathcal{B}(\psi(2S) \to \mu^+\mu^-)}\,. \tag{2}$$

The signal yields are extracted in two steps. First, an unbinned extended maximum-likelihood fit to the dimuon mass distribution is performed to obtain the $J/\psi$ and $\psi(2S)$ yields within the $J/\psi$ and $\psi(2S)$ mass windows, respectively. The nonresonant background yield, mostly due to $\gamma\gamma \to \mu^+\mu^-$ process, is also obtained from the mass fit. This fit uses

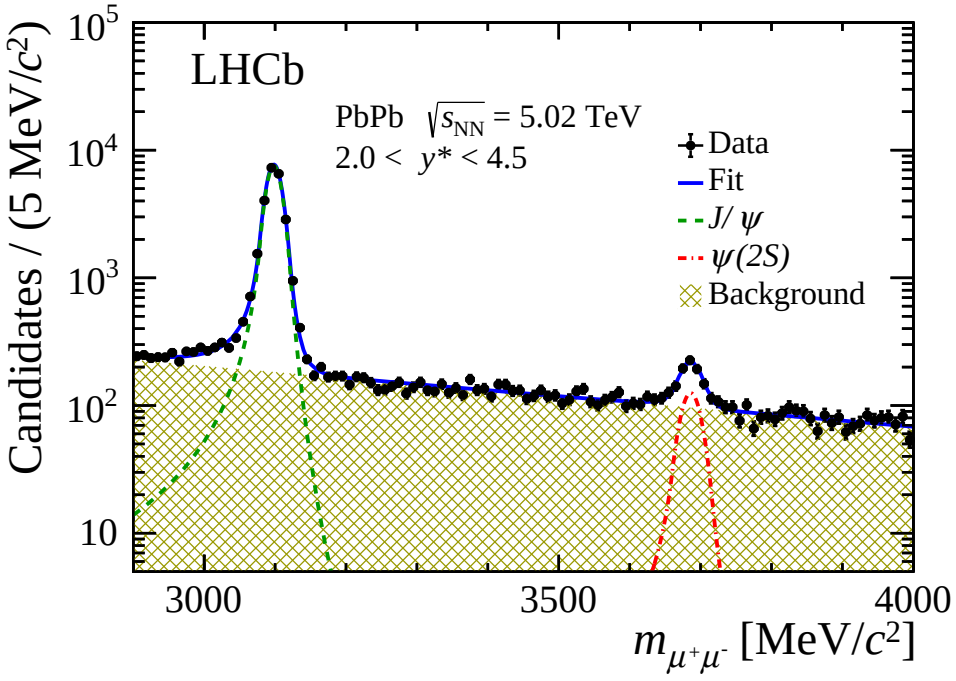


Figure 2: Dimuon mass distribution for signal candidates in the rapidity range $2.0 < y^* < 4.5$. The data are overlaid with the result of the fit.

double-sided Crystal-Ball functions to describe the $J/\psi$ and $\psi(2S)$ mass shapes and an exponential function for the nonresonant background. The fit is performed in the range $2.9 < m_{\mu^+\mu^-} < 4.0\,\text{GeV}/c^2$. The mass distribution and the corresponding fit are shown in Fig. 2.

In the second step, the coherent yields are determined with unbinned maximum-likelihood fits to the $\ln(p_{\text{T}}^{*2})$ distributions separately for the candidates inside the $J/\psi$ and $\psi(2S)$ mass windows. The yields of $J/\psi$ production include contributions from coherent and incoherent production, and feed-down from $\psi(2S)$ decays into $J/\psi$ ($\psi(2S) \to J/\psi X$). Similarly, the $\psi(2S)$ yields include contributions from both coherent and incoherent production, while the feed-down contribution from higher-order charmonium excited states is negligible given the current statistical precision. The quantity $\ln(p_{\text{T}}^{*2})$ is used because the variable $p_{\text{T}}^2$ is a proxy for the typical momentum exchange, $|t| \approx p_{\text{T}}^2$, in an elastic scattering process, and the logarithmic distribution allows one to see the peak of the data at low exchanged momenta. The coherent production has the smallest momentum exchange by definition, while the incoherent production gives a relatively larger transverse momentum to the $J/\psi$ or $\psi(2S)$ meson to balance the break-up of the pomeron-emitting nucleus. The feed-down contribution to $J/\psi$ production also has greater transverse momentum than the coherent production to balance the other products from the $\psi(2S)$ decay. The $\ln(p_{\text{T}}^{*2})$ shapes of coherent, incoherent and $\psi(2S)$ feed-down components are taken from STARLIGHT simulation, while the normalisation of these components are left free in the fit. The nonresonant background consists mostly of the $\gamma\gamma \to \mu^+\mu^-$ process with a slightly lower transverse momentum of the dimuon system than coherent charmonium production. The distribution also contains a small contribution

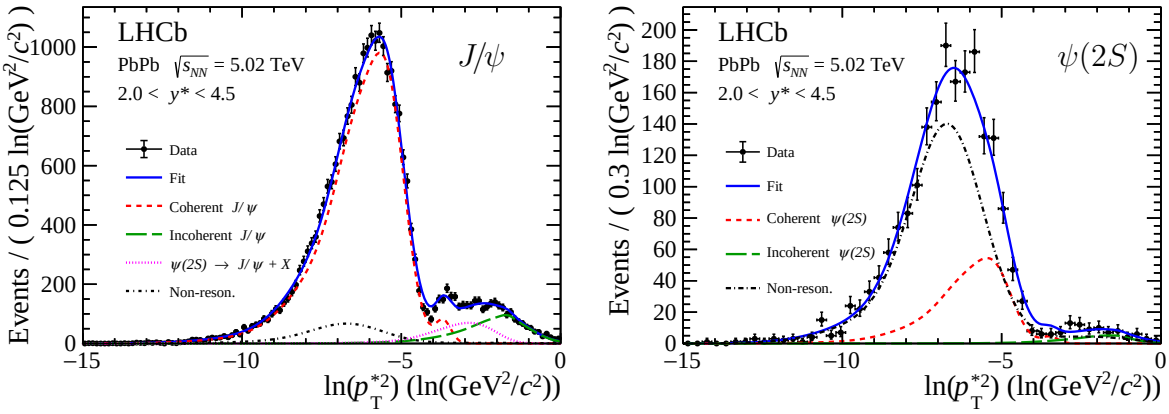


Figure 3: The $\ln(p_{\mathrm{T}}^{*2})$ distribution of dimuon candidates in the $2.0 < y^* < 4.5$ range for (left) $J/\psi$ candidates and (right) $\psi(2S)$ candidates. The data are overlaid with the result of the fit.

from the random pairing of uncorrelated muons produced in the hadronic interactions during peripheral or central lead-lead collisions, signified by a large transverse momentum of the dimuon system. The STARLIGHT simulation gives a precise description of $\ln(p_{\mathrm{T}}^{*2})$ spectrum of the $\gamma\gamma \to \mu^+\mu^-$ process, but not of the background from hadronic interactions. Instead, a data-driven method is chosen to model the nonresonant background by taking the dimuon candidates in the mass range $3.2 < m_{\mu^+\mu^-} < 3.6\,\mathrm{GeV}/c^2$ outside charmonium mass windows. In this way, the model includes the $\gamma\gamma \to \mu^+\mu^-$ process and the QCD background together, and gives an unbiased modelling of the $\ln(p_{\mathrm{T}}^{*2})$ spectrum. The yields of the nonresonant background are determined as the integral of the nonresonant component from the dimuon mass fit separately in the $J/\psi$ and $\psi(2S)$ mass windows, and are fixed in the $\ln(p_{\mathrm{T}}^{*2})$ fits.

Figure 3 shows the $\ln(p_{\mathrm{T}}^{*2})$ distributions of selected $J/\psi$ and $\psi(2S)$ candidates in the rapidity interval $2 < y^* < 4.5$. Fits to the $\ln(p_{\mathrm{T}}^{*2})$ distributions are performed in each $y^*$ interval to extract the corresponding $J/\psi$ and $\psi(2S)$ yields, as reported in Table 1. The coherent yield of $J/\psi$ and $\psi(2S)$ production for each $p_{\mathrm{T}}^*$ interval is calculated by subtracting the background components from the measured yield for that interval as reported in Tables 2 and 3. The contributions from background components are determined by an overall fit to the $\ln(p_{\mathrm{T}}^{*2})$ distributions.

Table 1: Total and coherent $J/\psi$ and $\psi(2S)$ yields from the invariant mass and transverse momentum fits in different rapidity intervals.

| Interval | $N_{J/\psi}^{\mathrm{tot}}$ | $N_{J/\psi}^{\mathrm{coh}}$ | $N_{\psi(2S)}^{\mathrm{tot}}$ | $N_{\psi(2S)}^{\mathrm{coh}}$ |
|---|---|---|---|---|
| $2.0 < y^* < 4.5$ | $23\,355 \pm 183$ | $20\,193 \pm 199$ | $513 \pm 43$ | $471 \pm 44$ |
| $2.0 < y^* < 2.5$ | $2\,457 \pm 60$ | $2\,070 \pm 66$ | $75 \pm 15$ | $65 \pm 15$ |
| $2.5 < y^* < 3.0$ | $6\,845 \pm 100$ | $5\,926 \pm 108$ | $147 \pm 26$ | $137 \pm 26$ |
| $3.0 < y^* < 3.5$ | $7\,875 \pm 106$ | $6\,883 \pm 115$ | $168 \pm 26$ | $161 \pm 26$ |
| $3.5 < y^* < 4.0$ | $5\,019 \pm 82$ | $4\,362 \pm 90$ | $102 \pm 18$ | $85 \pm 18$ |
| $4.0 < y^* < 4.5$ | $1\,166 \pm 38$ | $956 \pm 44$ | $24 \pm 8$ | $21 \pm 8$ |

The total efficiency $\varepsilon_{\text{tot}}$ is determined as the product of the acceptance efficiency ($\varepsilon_{\text{acc}}$), the muon acceptance efficiency ($\varepsilon_{\mu\text{-acc}}$), the tracking efficiency ($\varepsilon_{\text{trk}}$), the selection efficiency ($\varepsilon_{\text{sel}}$), the particle identification (PID) efficiency ($\varepsilon_{\text{PID}}$), the trigger efficiency ($\varepsilon_{\text{trg}}$) and the HERSCHEL-veto efficiency ($\varepsilon_{\text{her}}$). Each efficiency is evaluated separately for $J/\psi$ and $\psi(2S)$ mesons in each $y^*$ and $p_{\text{T}}^*$ interval for the differential cross-section measurements. Efficiencies are evaluated from simulation calibrated to data. The value of $\varepsilon_{\mu\text{-acc}}$ is determined at generator level as the fraction of events with both muon candidates passing $p_{\text{T}} > 700\,\text{MeV}/c$ and $2.0 < \eta < 4.5$. The signal candidates are required to pass the $p_{\text{T}} < 1\,\text{GeV}/c$ selection and fall in the mass windows defined in Sec. 3, for $J/\psi$ and $\psi(2S)$ mesons separately. For $\varepsilon_{\text{trk}}$, $\varepsilon_{\text{PID}}$ and $\varepsilon_{\text{trg}}$, the simulation does not always describe the data well. Efficiency corrections from data using the tag-and-probe method [24] are determined from $J/\psi$ events in PbPb collision data. The HERSCHEL-veto criteria is chosen to retain a signal efficiency of 90% according to a set of separately selected pure signal and background data samples. Dependencies of the efficiency correction on $y^*$ and $p_{\text{T}}^*$ of the dimuon system are studied and found to be negligible in the invariant mass range from 2.9 to $4.0\,\text{GeV}/c^2$.

Table 2: Total and coherent $J/\psi$ yields in different $p_{\text{T}}^*$ intervals within the rapidity range $2.0 < y^* < 4.5$.

| Interval [MeV/$c$] | $N_{J/\psi}^{\text{tot}}$ | $N_{J/\psi}^{\text{coh}}$ |
|---|---|---|
| $0 < p_{\text{T}}^* < 200$ | $21\,153 \pm 175$ | $20\,180 \pm 175$ |
| $0 < p_{\text{T}}^* < 20$ | $2\,216 \pm 58$ | $2\,204 \pm 58$ |
| $20 < p_{\text{T}}^* < 40$ | $5\,647 \pm 92$ | $5\,619 \pm 92$ |
| $40 < p_{\text{T}}^* < 60$ | $5\,931 \pm 83$ | $5\,885 \pm 83$ |
| $60 < p_{\text{T}}^* < 80$ | $3\,928 \pm 65$ | $3\,863 \pm 65$ |
| $80 < p_{\text{T}}^* < 100$ | $1\,848 \pm 44$ | $1\,759 \pm 44$ |
| $100 < p_{\text{T}}^* < 120$ | $497 \pm 23$ | $381 \pm 24$ |
| $120 < p_{\text{T}}^* < 140$ | $225 \pm 16$ | $88 \pm 17$ |
| $140 < p_{\text{T}}^* < 160$ | $289 \pm 17$ | $137 \pm 18$ |
| $160 < p_{\text{T}}^* < 180$ | $328 \pm 18$ | $167 \pm 20$ |
| $180 < p_{\text{T}}^* < 200$ | $244 \pm 16$ | $77 \pm 17$ |

# 5 Systematic uncertainties

Systematic uncertainties on the cross-section measurements arise from the efficiency and background determination, signal and background shapes, momentum resolution, integrated luminosity and knowledge of the $J/\psi \to \mu^+\mu^-$ and $\psi(2S) \to \mu^+\mu^-$ branching fractions. For the $\psi(2S)$ to $J/\psi$ cross-section ratio measurement, only systematic uncertainties from the charmonia decay branching fractions are considered. Those from efficiency and background determination, signal and background shapes integrated luminosity are highly correlated and cancel. A summary of the systematic uncertainties is presented in Table 4.

Table 3: Total and coherent $\psi(2S)$ yields in different $p_{\mathrm{T}}^{*}$ intervals within the rapidity range $2.0 < y^{*} < 4.5$.

| Interval [MeV/$c$] | $N_{\psi(2S)}^{\mathrm{tot}}$ | $N_{\psi(2S)}^{\mathrm{coh}}$ |
|---|---|---|
| $0 < p_{\mathrm{T}}^{*} < 200$ | $475 \pm 41$ | $468 \pm 41$ |
| $0 < p_{\mathrm{T}}^{*} < 30$ | $77 \pm 35$ | $77 \pm 35$ |
| $30 < p_{\mathrm{T}}^{*} < 70$ | $275 \pm 39$ | $274 \pm 39$ |
| $70 < p_{\mathrm{T}}^{*} < 90$ | $91 \pm 14$ | $91 \pm 14$ |
| $90 < p_{\mathrm{T}}^{*} < 110$ | $27 \pm 8$ | $27 \pm 8$ |
| $110 < p_{\mathrm{T}}^{*} < 150$ | $0 \pm 5$ | $0 \pm 5$ |
| $150 < p_{\mathrm{T}}^{*} < 200$ | $5 \pm 4$ | $2 \pm 4$ |

The systematic uncertainties related to the efficiencies are driven by the sizes of the simulation and data samples. They vary from (0.5 – 2.0)% for the tracking efficiency, (0.9 – 1.6)% for the PID efficiency and (2.1 – 3.7)% for the trigger efficiency, across different $y^{*}$ and $p_{\mathrm{T}}^{*}$ intervals. The uncertainty associated with the HERSCHEL efficiency is a constant 1.4%.

The uncertainty on the background shape is estimated by varying the shape parameters within their fitted uncertainties. The maximum difference on the extracted signal yields is 1.2%, and is assigned as the background uncertainty.

The momentum resolution is expected to shift events from one $p_{\mathrm{T}}^{*}$ interval to another. The uncertainties due to the momentum resolution are evaluated by comparing the $p_{\mathrm{T}}$ spectra between generated and reconstructed events. The evaluated relative uncertainties vary from 0.9 to 34% for different $p_{\mathrm{T}}^{*}$ intervals. The largest uncertainty corresponds to the $p_{\mathrm{T}}^{*}$ interval between 140 to 160 MeV as shown in Table 8 (Appendix A), where very small signal yields are observed.

The slight discrepancies between the data and the fit results are visible at $\ln(p_{\mathrm{T}}^{*2}) \sim -4\,[\ln(\,\mathrm{GeV}/c^{2})]$ for both the $J/\psi$ and $\psi(2S)$ fits, as seen in Fig. 3. This is expected to originate from a mis-modelling of the predicted signal shape from simulation. A systematic uncertainty on the signal shape model is estimated by evaluating the difference between the fitted signal yields with respect to an alternative empirical signal shape. The obtained difference is about 0.04%, negligible compared to other uncertainties shown in Table 4.

The uncertainties on the branching fractions result in relative uncertainties on the measured cross-sections of 0.6% and 2.1% [23], respectively. The relative uncertainty on the luminosity is 4.4% [25].

# 6 Results and discussion

The integrated cross-sections of coherent $J/\psi$ and $\psi(2S)$ photoproduction in PbPb collisions are measured in the rapidity region $2.0 < y^{*} < 4.5$ as

$$\sigma_{J/\psi}^{\mathrm{coh}} = 5.965 \pm 0.059 \pm 0.232 \pm 0.262\,\mathrm{mb}\,,$$
$$\sigma_{\psi(2S)}^{\mathrm{coh}} = 0.923 \pm 0.086 \pm 0.028 \pm 0.040\,\mathrm{mb}\,,$$

Table 4: Summary of the systematic uncertainties.

| Source | Relative uncertainty [%] | |
|---|---|---|
| | $\sigma^{\mathrm{coh}}_{J/\psi}$ | $\sigma^{\mathrm{coh}}_{\psi(2S)}$ |
| Tracking efficiency | 0.5–2.0 | 0.5–2.0 |
| PID efficiency | 0.9–1.6 | 0.9–1.6 |
| Trigger efficiency | 2.7–3.7 | 2.1–2.5 |
| HERSCHEL efficiency | 1.4 | 1.4 |
| Background estimation | 1.2 | 1.2 |
| Momentum resolution | 0.9–34 | 1.3–27 |
| Branching fraction | 0.6 | 2.1 |
| Luminosity | 4.4 | 4.4 |

where the first listed uncertainty is statistical, the second is systematic and the third is due to the luminosity determination. The cross-section ratio between coherent $\psi(2S)$ and $J/\psi$ photoproduction is measured to be

$$\sigma^{\mathrm{coh}}_{\psi(2S)}/\sigma^{\mathrm{coh}}_{J/\psi} = 0.155 \pm 0.014 \pm 0.003\,,$$

where the first uncertainty is statistical and the second is systematic. The luminosity uncertainty cancels in the ratio measurement.

The measured differential cross-sections for coherent $J/\psi$ and $\psi(2S)$ photoproduction as functions of $y^*$ and $p^*_{\mathrm{T}}$ are shown in Figs. 4 and 5, respectively. The cross-section ratio of coherent photoproduction between $\psi(2S)$ and $J/\psi$ as a function of rapidity is shown in Fig. 6. The data are shown as black points with black error bars for the statistical uncertainties, red boxes show the systematic uncertainties and the fully correlated uncertainty due to integrated luminosity is labelled separately. In the same figures, the results are compared to several theoretical predictions. The numerical values of the results are reported in Tables 5 – 9 in Appendix A.

The STARLIGHT prediction is based on the concept of vector meson dominance with parameters tuned according to previous UPC data [16]. As shown in Figs. 4 and 5, it gives a good description of the decreasing slope as a function of $y^*$ and the shape as a function of $p^*_{\mathrm{T}}$, but the overall predicted normalisation is about 20% and 50% higher for $J/\psi$ and $\psi(2S)$ production, respectively. The ratio between $\psi(2S)$ and $J/\psi$ production in Fig. 6 is also well modelled within data uncertainties.

Two sets of calculations using leading-order perturbative QCD (LO pQCD) are provided by Guzey, Kryshen, Strikman and Zhalov [12, 26] (GKSZ) for both $J/\psi$ and $\psi(2S)$ coherent photoproduction. One uses the leading twist approximation (LTA) [27] to model the nuclear shadowing effect in the initial state. The shaded area labelled "LTA" in Fig. 4 corresponds to the uncertainties on the nuclear shadowing determined in Ref. [27]. The other uses EPS09 nuclear parton distribution functions (nPDFs) [28] for the nuclear shadowing, with an error band labelled "nPDF unce." under "EPS09" in Fig. 4 presenting the uncertainties of the nuclear modification. Note that the two LO pQCD calculations carry *ad hoc* normalisation factors of the cross-section determined using high-energy HERA data [12, 29]. Both of them predict well the shapes of the data

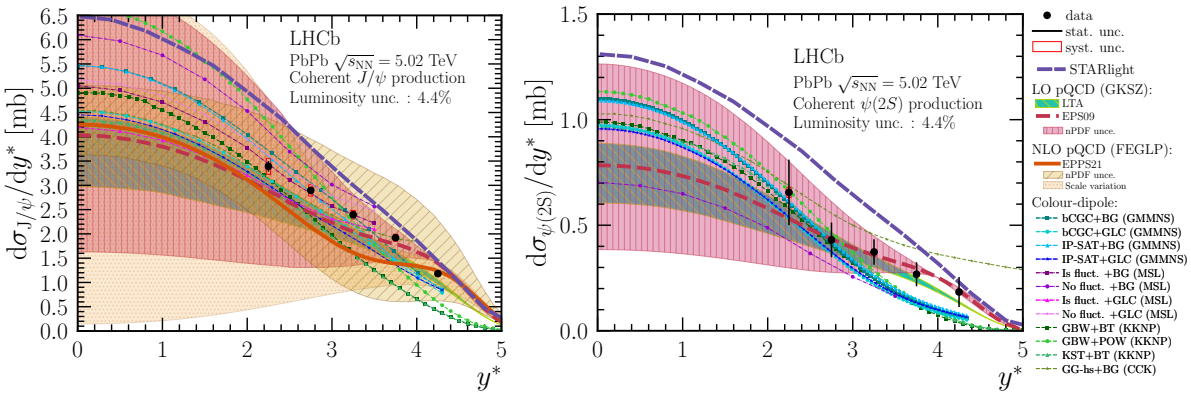


Figure 4: Differential cross-section as a function $y^*$ for coherent (left) $J/\psi$ and (right) $\psi(2S)$ photoproduction, compared to theoretical predictions.

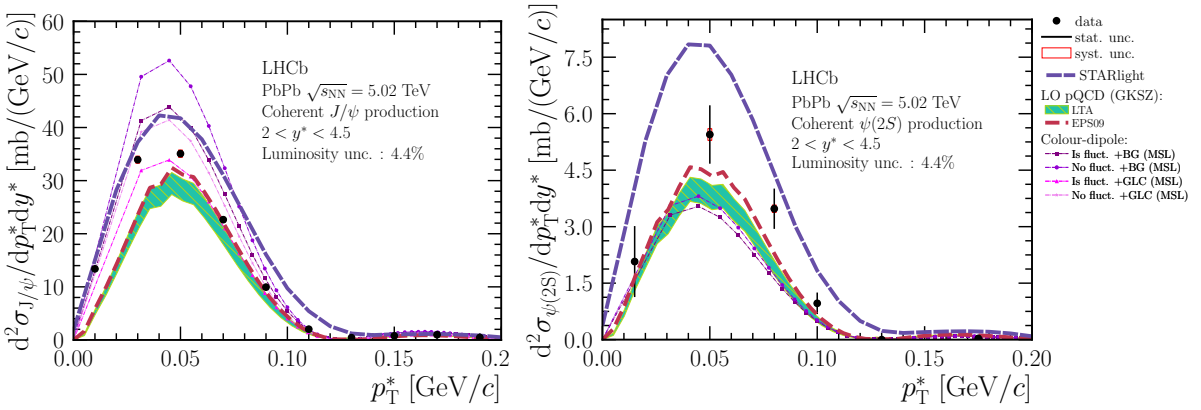


Figure 5: Differential cross-section as a function of $p_T^*$ within the rapidity range $2 < y^* < 4.5$ for coherent (left) $J/\psi$ and (right) $\psi(2S)$ photoproduction compared to theoretical predictions.

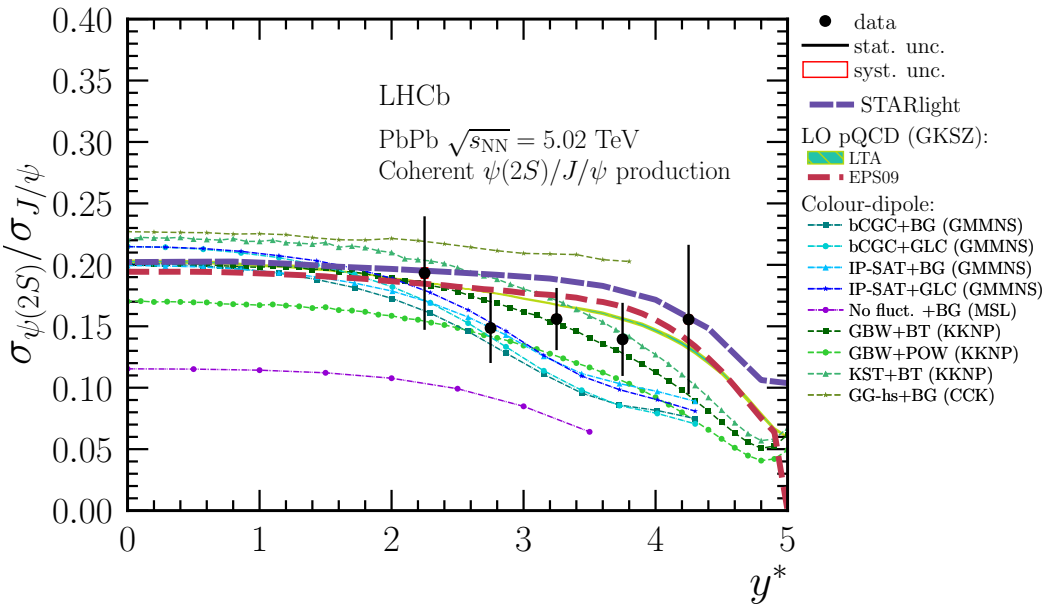


Figure 6: Differential cross-section ratio of $\psi(2S)$ to $J/\psi$ coherent photoproduction as a function of $y^*$, compared to theoretical predictions.

for both $J/\psi$ and $\psi(2S)$ production as a function of $y^*$ in Fig. 4. A slightly larger (smaller) $p_{\mathrm{T}}^*$ is predicted for $J/\psi$ ($\psi(2S)$) production than the data in Fig. 5. An underestimation of about 15% of the normalisation can be seen for both $J/\psi$ and $\psi(2S)$ production, but the ratio is well modelled in Fig. 6. The large nPDF uncertainties in Fig. 4 indicate that coherent charmonium photoproduction in heavy ion collisions is very sensitive to the nuclear modification factors, especially to the modelling of the gluon shadowing, used in the LO pQCD calculations [12].

The next-to-leading-order (NLO) pQCD calculation using the most recent EPPS21 NLO nPDFs [30] is provided by Flett, Eskola, Guzey, Löytäinen and Paukkunen [31] (FEGLP), and is only available for $J/\psi$ production as shown in the left plot of Fig. 4. This is the first pQCD calculation without using *ad hoc* normalisation factors of the cross-section compared to previous LO calculations. The predicted central value is about $15-20\%$ lower than the data, which is calculated based on a factorization/renormalisation scale, $\mu = 0.76\, m_{J/\psi} = 2.37\,\mathrm{GeV}$, tuned using previous ALICE [8, 9, 32, 33], LHCb [7] and CMS [6] data. The substantial shaded area labelled "scale variation" corresponds to a variation of $\mu$ from $m_{J/\psi}/2$ to $m_{J/\psi}$, indicating that the cross-section is extremely sensitive to the missing higher-order pQCD corrections. The nPDF uncertainties are much smaller for rapidity below 2 but much bigger for rapidity greater than 3 in the NLO pQCD calculation compared to the LO calculation. This is understood as an interplay of the real and imaginary parts of the quark and gluon amplitudes that causes a certain level of mutual cancellation of the nuclear effects, especially at lower rapidity region [31]. High-precision data can nevertheless help to further understand these effects.

Various calculations within the framework of the colour-dipole model [11, 34–39] are also compared in Fig. 4 for both $J/\psi$ (left) and $\psi(2S)$ (right). All these models inherit parameters determined by previous HERA data [3, 4, 29].

The calculations provided by Gonçalves, Machado, Moreira, Navarra, Sampaio dos Santos [36, 37] (GMMNS) employ the impact-parameter-color-gluon-condensate (bCGC) [40, 41] and the impact-parameter-saturation (IP-SAT) [42] parameterisations for the dipole-proton cross-section, combined with boosted Gaussian (BG) and Gaussian-light-cone (GLC) models [36] of the vector-meson wave functions. They agree with the $J/\psi$ data reasonably well for rapidity below 3, while an underestimation of about 10–30% can be observed in Figs. 4 and 5 for rapidity above 3.5 in the case of $J/\psi$, and about 20–60% for rapidity above 3 for $\psi(2S)$. This results in a systematic suppression of the ratio between $\psi(2S)$ and $J/\psi$ for rapidity above 3 as seen in Fig. 6.

Predictions calculated by Mäntysaari, Schenke and Lappi [38,39] (MSL) use the IP-SAT parameterisation to describe the dipole-proton cross-section but include sub-nucleon scale fluctuations. Calculations with (Is fluct.) and without (No fluct.) sub-nucleon fluctuation together with BG or GLC vector-meson wave functions are compared to the measurements in Figs. 4 and 5. Only the No fluct.+BG calculation is available for $\psi(2S)$ as a function of $y^*$ and only No fluct.+BG and Is fluct.+BG are available for $\psi(2S)$ as a function of $p_{\mathrm{T}}^*$. They predict well the shapes of the $J/\psi$ differential cross-section as functions of $y^*$ and $p_{\mathrm{T}}^*$, but the predicted $p_{\mathrm{T}}^*$ for $\psi(2S)$ production is slightly smaller than the data. Variations in the normalisation are relatively large among these models. The two models using BG vector-meson wave functions predict higher normalisation than the two using GLC. Because these models are calculated for rapidity below 3.5, the normalisation of the predictions as a function of $p_{\mathrm{T}}^*$ appears relatively lower than that as a function of $y^*$. Calculations for $\psi(2S)$ are relatively worse than for $J/\psi$ because we know less about the

$\psi(2S)$ wave function than $J/\psi$ [10, 39, 40], the precise data can nevertheless be helpful to improve this aspect. Among them, Is fluct.+BG gives the best prediction for $J/\psi$ as a function of $y^*$.

Models by Kopeliovich, Krelina, Nemchik and Potashnikova [35] (KKNP) are composed of quarkonium wave functions determined by the Buchmüller–Tye (BT) [43] or power-like (POW) [44, 45] potentials, as well as the Golec–Biernat–Wusthoff (GBW) [46, 47] or Kopeliovich–Schafer–Tarasov (KST) [48] models for the dipole-nucleon cross-sections. They appear similar to the models provided by GMMNS, with reasonably good agreement for $J/\psi$ production for $y^* < 3$, but with an overestimation of the decreasing slope, and consequently an underestimation of the data of 20–60% for $y^* > 3$ for $\psi(2S)$ production. But the decreasing slopes are consistent between the $J/\psi$ and $\psi(2S)$ calculations so that the predicted ratio between the two agrees well with the data.

In an alternative approach (GG-hs+BG) by Cepila, Contreras and Krelina [34] (CCK), the BG model is used for the vector-meson wave function, and the dipole-nucleon cross-section is parameterised assuming the nucleon is composed of so-called hot-spots (hs), regions with high-gluon density. The standard Glauber-Gribov (GG) formalism [49–51] is then used to extend the dipole-nucleon cross-section to the case for dipole-nucleus. This model describes well the slope as a function of $y^*$ for both $J/\psi$ and $\psi(2S)$ data, but a relatively large overestimation of the normalisation for $\psi(2S)$ production. The corresponding prediction for the ratio between $\psi(2S)$ and $J/\psi$ production is therefore relatively higher than the data points.

In a closer look at the differential cross-section as a function of rapidity in Fig. 4 for both $J/\psi$ and $\psi(2S)$ mesons, one can observe that the data do not consistently decrease at a fixed slope, instead it has a subtle and elusive bump between 3 and 4. This is the first observation of this subtle signature thanks to the high precision data. Among the models discussed above, only the standard pQCD calculations can reproduce this feature, and can be understood as an interplay of the real and imaginary parts of the quark and gluon amplitudes [12, 31].

# 7 Conclusion

The coherent (exclusive) $J/\psi$ and $\psi(2S)$ photoproduction cross-sections in PbPb ultra-peripheral collisions at a centre-of-mass energy of $\sqrt{s_{\rm NN}} = 5.02\,\text{TeV}$ are studied using a data sample corresponding to an integrated luminosity of $228 \pm 10\,\mu\text{b}^{-1}$ collected by the LHCb detector. The differential cross-sections, as a function of $y^*$ and $p_{\rm T}^*$, are measured separately for $J/\psi$ and $\psi(2S)$ mesons in the ranges $2.0 < y^* < 4.5$ and $0 < p_{\rm T}^* < 0.2\,\text{GeV}/c$. The ratio of the cross-sections between the coherent $\psi(2S)$ and $J/\psi$ production, as a function of rapidity, is also determined for the first time in PbPb collisions and is found to be compatible with theoretical models. The $J/\psi$ results are the most precise measurement to date, while the $\psi(2S)$ results represent the first measurement in the forward region.

# Acknowledgements

We express our gratitude to our colleagues in the CERN accelerator departments for the excellent performance of the LHC. We thank the technical and administrative staff at the LHCb institutes. We acknowledge support from CERN and from the national agencies:

CAPES, CNPq, FAPERJ and FINEP (Brazil); MOST and NSFC (China); CNRS/IN2P3 (France); BMBF, DFG and MPG (Germany); INFN (Italy); NWO (Netherlands); MNiSW and NCN (Poland); MEN/IFA (Romania); MICINN (Spain); SNSF and SER (Switzerland); NASU (Ukraine); STFC (United Kingdom); DOE NP and NSF (USA). We acknowledge the computing resources that are provided by CERN, IN2P3 (France), KIT and DESY (Germany), INFN (Italy), SURF (Netherlands), PIC (Spain), GridPP (United Kingdom), CSCS (Switzerland), IFIN-HH (Romania), CBPF (Brazil), Polish WLCG (Poland) and NERSC (USA). We are indebted to the communities behind the multiple open-source software packages on which we depend. Individual groups or members have received support from ARC and ARDC (Australia); Minciencias (Colombia); AvH Foundation (Germany); EPLANET, Marie Skłodowska-Curie Actions and ERC (European Union); A*MIDEX, ANR, IPhU and Labex P2IO, and Région Auvergne-Rhône-Alpes (France); Key Research Program of Frontier Sciences of CAS, CAS PIFI, CAS CCEPP, Fundamental Research Funds for the Central Universities, and Sci. & Tech. Program of Guangzhou (China); GVA, XuntaGal, GENCAT and Prog. Atracción Talento, CM (Spain); SRC (Sweden); the Leverhulme Trust, the Royal Society and UKRI (United Kingdom).

# Appendices

# A Numerical results

Table 5: The differential cross-section for coherent $J/\psi$ production as a function of $y^*$.

| Interval | $\mathrm{d}\sigma^{\mathrm{coh}}_{J/\psi}/\mathrm{d}y^*$ [mb] | Uncertainties [mb] | | | |
|---|---|---|---|---|---|
| | | Stat. | Syst. | Lumi. | Total |
| $2.0 < y^* < 2.5$ | 3.392 | 0.108 | 0.165 | 0.147 | 0.247 |
| $2.5 < y^* < 3.0$ | 2.896 | 0.053 | 0.117 | 0.127 | 0.181 |
| $3.0 < y^* < 3.5$ | 2.395 | 0.040 | 0.089 | 0.105 | 0.144 |
| $3.5 < y^* < 4.0$ | 1.922 | 0.039 | 0.072 | 0.084 | 0.117 |
| $4.0 < y^* < 4.5$ | 1.181 | 0.054 | 0.049 | 0.052 | 0.089 |
| $2.0 < y^* < 4.5$ | 5.965 | 0.059 | 0.232 | 0.262 | 0.355 |

Table 6: The differential cross-section of coherent $\psi(2S)$ production as a function of $y^*$.

| Interval | $\mathrm{d}\sigma^{\mathrm{coh}}_{\psi(2S)}/\mathrm{d}y^*$ [mb] | Uncertainties [mb] | | | |
|---|---|---|---|---|---|
| | | Stat. | Syst. | Lumi. | Total |
| $2.0 < y^* < 2.5$ | 0.656 | 0.155 | 0.024 | 0.029 | 0.160 |
| $2.5 < y^* < 3.0$ | 0.430 | 0.082 | 0.014 | 0.019 | 0.085 |
| $3.0 < y^* < 3.5$ | 0.373 | 0.060 | 0.012 | 0.016 | 0.064 |
| $3.5 < y^* < 4.0$ | 0.268 | 0.057 | 0.009 | 0.012 | 0.059 |
| $4.0 < y^* < 4.5$ | 0.184 | 0.071 | 0.007 | 0.008 | 0.072 |
| $2.0 < y^* < 4.5$ | 0.923 | 0.086 | 0.028 | 0.040 | 0.099 |

Table 7: The differential cross-section ratio between $\psi(2S)$ and $J/\psi$ coherent production as a function of $y^*$. The uncertainty due to luminosity determination cancels in the ratio.

| Interval | $\mathrm{d}\sigma^{\mathrm{coh}}_{\psi(2S)}/\mathrm{d}\sigma^{\mathrm{coh}}_{J/\psi}$ | Uncertainties | | |
|---|---|---|---|---|
| | | Stat. | Syst. | Total |
| $2.0 < y^* < 2.5$ | 0.193 | 0.046 | 0.004 | 0.046 |
| $2.5 < y^* < 3.0$ | 0.149 | 0.028 | 0.003 | 0.029 |
| $3.0 < y^* < 3.5$ | 0.156 | 0.025 | 0.003 | 0.026 |
| $3.5 < y^* < 4.0$ | 0.139 | 0.030 | 0.003 | 0.030 |
| $4.0 < y^* < 4.5$ | 0.156 | 0.061 | 0.003 | 0.061 |
| $2.0 < y^* < 4.5$ | 0.155 | 0.014 | 0.003 | 0.015 |

Table 8: The double differential cross-section of coherent $J/\psi$ production as a function of $p_{\mathrm{T}}^{*}$ in rapidity range $2.0 < y^{*} < 4.5$.

| Interval [ MeV/$c$] | $\mathrm{d}^2\sigma^{\mathrm{coh}}_{J/\psi}/\mathrm{d}p_{\mathrm{T}}^{*}\mathrm{d}y^{*}$ [mb/(GeV/$c$)] | Uncertainties [mb/(GeV/$c$)] | | | |
|---|---|---|---|---|---|
| | | Stat. | Syst. | Lumi. | Total |
| $0 < p_{\mathrm{T}}^{*} < 20$ | 13.391 | 0.352 | 0.908 | 0.587 | 1.138 |
| $20 < p_{\mathrm{T}}^{*} < 40$ | 33.940 | 0.556 | 2.007 | 1.489 | 2.560 |
| $40 < p_{\mathrm{T}}^{*} < 60$ | 35.077 | 0.495 | 1.462 | 1.538 | 2.179 |
| $60 < p_{\mathrm{T}}^{*} < 80$ | 22.645 | 0.381 | 0.492 | 0.993 | 1.172 |
| $80 < p_{\mathrm{T}}^{*} < 100$ | 9.945 | 0.249 | 0.472 | 0.436 | 0.689 |
| $100 < p_{\mathrm{T}}^{*} < 120$ | 2.028 | 0.128 | 0.311 | 0.089 | 0.347 |
| $120 < p_{\mathrm{T}}^{*} < 140$ | 0.432 | 0.083 | 0.138 | 0.019 | 0.163 |
| $140 < p_{\mathrm{T}}^{*} < 160$ | 0.781 | 0.103 | 0.273 | 0.034 | 0.293 |
| $160 < p_{\mathrm{T}}^{*} < 180$ | 0.986 | 0.118 | 0.213 | 0.043 | 0.247 |
| $180 < p_{\mathrm{T}}^{*} < 200$ | 0.464 | 0.102 | 0.080 | 0.020 | 0.131 |
| $0 < p_{\mathrm{T}}^{*} < 200$ | 11.904 | 0.103 | 0.233 | 0.522 | 0.581 |

Table 9: The double differential cross-section of coherent $\psi(2S)$ production as a function of $p_{\mathrm{T}}^{*}$ in rapidity range $2.0 < y^{*} < 4.5$.

| Interval [ MeV/$c$] | $\mathrm{d}^2\sigma^{\mathrm{coh}}_{\psi(2S)}/\mathrm{d}p_{\mathrm{T}}^{*}\mathrm{d}y^{*}$ [mb/(GeV/$c$)] | Uncertainties [mb/(GeV/$c$)] | | | |
|---|---|---|---|---|---|
| | | Stat. | Syst. | Lumi. | Total |
| $0 < p_{\mathrm{T}}^{*} < 30$ | 2.073 | 0.942 | 0.141 | 0.091 | 0.957 |
| $30 < p_{\mathrm{T}}^{*} < 70$ | 5.447 | 0.775 | 0.254 | 0.239 | 0.850 |
| $70 < p_{\mathrm{T}}^{*} < 90$ | 3.476 | 0.535 | 0.110 | 0.152 | 0.567 |
| $90 < p_{\mathrm{T}}^{*} < 110$ | 1.136 | 0.337 | 0.108 | 0.050 | 0.357 |
| $110 < p_{\mathrm{T}}^{*} < 150$ | 0.000 | 0.093 | 0.000 | 0.000 | 0.093 |
| $150 < p_{\mathrm{T}}^{*} < 200$ | 0.025 | 0.051 | 0.006 | 0.001 | 0.051 |
| $0 < p_{\mathrm{T}}^{*} < 200$ | 1.833 | 0.160 | 0.052 | 0.080 | 0.187 |

# References


[1] C. A. Bertulani, S. R. Klein, and J. Nystrand, *Physics of ultra-peripheral nuclear collisions*, Ann. Rev. Nucl. Part. Sci. **55** (2005) 271, arXiv:nucl-ex/0502005.

[2] S. P. Jones, A. D. Martin, M. G. Ryskin, and T. Teubner, *Exclusive $J/\psi$ and $\Upsilon$ photoproduction and the low x gluon*, J. Phys. **G43** (2016) 035002, arXiv:1507.06942.

[3] H1 collaboration, A. Aktas *et al.*, *Elastic J/psi production at HERA*, Eur. Phys. J. **C46** (2006) 585, arXiv:hep-ex/0510016.

[4] ZEUS collaboration, S. Chekanov *et al.*, *Exclusive photoproduction of J / psi mesons at HERA*, Eur. Phys. J. **C24** (2002) 345, arXiv:hep-ex/0201043.

[5] PHENIX collaboration, S. Afanasiev *et al.*, *Photoproduction of J/psi and of high mass e+e- in ultra-peripheral Au+Au collisions at* $\sqrt{s_{NN}} = 200\,\text{GeV}$, Phys. Lett. **B679** (2009) 321, arXiv:0903.2041.

[6] CMS collaboration, V. Khachatryan *et al.*, *Coherent $J/\psi$ photoproduction in ultra-peripheral PbPb collisions at $\sqrt{s_{NN}} = 2.76$ TeV with the CMS experiment*, Phys. Lett. **B772** (2017) 489, arXiv:1605.06966.

[7] LHCb collaboration, R. Aaij *et al.*, *Study of coherent $J/\psi$ production in lead-lead collisions at $\sqrt{s_{NN}} = 5$ TeV*, JHEP **07** (2022) 117, arXiv:2107.03223.

[8] ALICE collaboration, S. Acharya *et al.*, *Coherent $J/\psi$ and $\psi'$ photoproduction at midrapidity in ultra-peripheral Pb-Pb collisions at $\sqrt{s_{NN}} = 5.02$ TeV*, Eur. Phys. J. **C81** (2021) 712, arXiv:2101.04577.

[9] ALICE collaboration, S. Acharya *et al.*, *Coherent $J/\psi$ photoproduction at forward rapidity in ultra-peripheral Pb-Pb collisions at $\sqrt{s_{NN}} = 5.02$ TeV*, Phys. Lett. **B798** (2019) 134926, arXiv:1904.06272.

[10] H. Kowalski, L. Motyka, and G. Watt, *Exclusive diffractive processes at HERA within the dipole picture*, Phys. Rev. **D74** (2006) 074016, arXiv:hep-ph/0606272.

[11] V. P. Gonçalves and M. V. T. Machado, *Vector meson production in coherent hadronic interactions: an update on predictions for RHIC and LHC*, Phys. Rev. **C84** (2011) 011902, arXiv:1106.3036.

[12] V. Guzey, E. Kryshen, and M. Zhalov, *Coherent photoproduction of vector mesons in ultraperipheral heavy ion collisions: Update for run2 at the CERN Large Hadron Collider*, Phys. Rev. **C93** (2016) 055206, arXiv:1602.01456.

[13] LHCb Collaboration, A. A. Alves Jr. *et al.*, *The LHCb detector at the LHC*, JINST **3** (2008) S08005.

[14] LHCb Collaboration, R. Aaij *et al.*, *LHCb detector performance*, Int. J. Mod. Phys. **A30** (2015) 1530022, arXiv:1412.6352.

[15] K. C. Akiba *et al.*, *The* HeRSCheL *detector: high-rapidity shower counters for LHCb*, JINST **13** (2018) P04017, arXiv:1801.04281.

[16] S. R. Klein *et al.*, *STARlight: A Monte Carlo simulation program for ultra-peripheral collisions of relativistic ions*, Comput. Phys. Commun. **212** (2017) 258, arXiv:1607.03838.

[17] I. Belyaev *et al.*, *Handling of the generation of primary events in Gauss, the LHCb simulation framework*, J. Phys. Conf. Ser. **331** (2011) 032047.

[18] D. J. Lange, *The EvtGen particle decay simulation package*, Nucl. Instrum. Meth. **A462** (2001) 152.

[19] N. Davidson, T. Przedzinski, and Z. Was, *PHOTOS interface in C++: Technical and physics documentation*, Comp. Phys. Comm. **199** (2016) 86, arXiv:1011.0937.

[20] Geant4 Collaboration, J. Allison *et al.*, *Geant4 developments and applications*, IEEE Trans. Nucl. Sci. **53** (2006) 270.

[21] Geant4 Collaboration, S. Agostinelli *et al.*, GEANT4*: A simulation toolkit*, Nucl. Instrum. Meth. **A506** (2003) 250.

[22] M. Clemencic *et al.*, *The LHCb simulation application, Gauss: Design, evolution and experience*, J. Phys. Conf. Ser. **331** (2011) 032023.

[23] Particle Data Group, P. A. Zyla *et al.*, *Review of particle physics*, Prog. Theor. Exp. Phys. **2020** (2020) 083C01.

[24] LHCb collaboration, R. Aaij *et al.*, *Measurement of the track reconstruction efficiency at LHCb*, JINST **10** (2015) P02007, arXiv:1408.1251.

[25] LHCb collaboration, R. Aaij *et al.*, *Precision luminosity measurements at LHCb*, JINST **9** (2014) P12005, arXiv:1410.0149.

[26] V. Guzey, M. Strikman, and M. Zhalov, *Accessing transverse nucleon and gluon distributions in heavy nuclei using coherent vector meson photoproduction at high energies in ion ultraperipheral collisions*, Phys. Rev. **C95** (2017) 025204, arXiv:1611.05471.

[27] L. Frankfurt, V. Guzey, and M. Strikman, *Leading twist nuclear shadowing phenomena in hard processes with nuclei*, Phys. Rept. **512** (2012) 255, arXiv:1106.2091.

[28] K. J. Eskola, H. Paukkunen, and C. A. Salgado, *EPS09: A new generation of NLO and LO nuclear parton distribution functions*, JHEP **04** (2009) 065, arXiv:0902.4154.

[29] ZEUS collaboration, M. Derrick *et al.*, *Measurement of elastic $\phi$ photoproduction at HERA*, Phys. Lett. **B377** (1996) 259, arXiv:hep-ex/9601009.

[30] K. J. Eskola, P. Paakkinen, H. Paukkunen, and C. A. Salgado, *EPPS21: a global QCD analysis of nuclear PDFs*, Eur. Phys. J. **C82** (2022) 413, arXiv:2112.12462.

[31] K. J. Eskola *et al.*, *Exclusive $J/\psi$ photoproduction in ultraperipheral Pb+Pb collisions at the CERN Large Hadron Collider calculated at next-to-leading order perturbative QCD*, Phys. Rev. **C106** (2022) 035202, arXiv:2203.11613.

[32] ALICE collaboration, B. Abelev *et al.*, *Coherent $J/\psi$ photoproduction in ultra-peripheral Pb-Pb collisions at $\sqrt{s_{NN}} = 2.76$ TeV*, Phys. Lett. **B718** (2013) 1273, arXiv:1209.3715.

[33] ALICE collaboration, E. Abbas *et al.*, *Charmonium and $e^+e^-$ pair photoproduction at mid-rapidity in ultra-peripheral Pb-Pb collisions at $\sqrt{s_{\rm NN}}$=2.76 TeV*, Eur. Phys. J. **C73** (2013) 2617, arXiv:1305.1467.

[34] J. Cepila, J. G. Contreras, and M. Krelina, *Coherent and incoherent* J/$\psi$ *photonuclear production in an energy-dependent hot-spot model*, Phys. Rev. **C97** (2018) 024901, arXiv:1711.01855.

[35] B. Z. Kopeliovich, M. Krelina, J. Nemchik, and I. K. Potashnikova, *Ultraperipheral nuclear collisions as a source of heavy quarkonia*, Phys. Rev. **D107** (2023) 054005, arXiv:2008.05116.

[36] V. P. Gonçalves *et al.*, *Color dipole predictions for the exclusive vector meson photoproduction in pp, p*Pb*, and* PbPb *collisions at run2 LHC energies*, Phys. Rev. **D96** (2017) 094027, arXiv:1710.10070.

[37] V. P. Gonçalves and M. V. T. Machado, *The QCD pomeron in ultraperipheral heavy ion collisions: IV. Photonuclear production of vector mesons*, Eur. Phys. J. **C40** (2005) 519, arXiv:hep-ph/0501099.

[38] H. Mäntysaari and B. Schenke, *Probing subnucleon scale fluctuations in ultraperipheral heavy ion collisions*, Phys. Lett. **B772** (2017) 832, arXiv:1703.09256.

[39] T. Lappi and H. Mäntysaari, *Diffractive vector meson production in ultraperipheral heavy ion collisions from the color glass condensate*, PoS **DIS2014** (2014) 069, arXiv:1406.2877.

[40] H. Kowalski, L. Motyka, and G. Watt, *Exclusive diffractive processes at HERA within the dipole picture*, Phys. Rev. **D74** (2006) 074016, arXiv:hep-ph/0606272.

[41] G. Watt and H. Kowalski, *Impact parameter dependent colour glass condensate dipole model*, Phys. Rev. D **78** (2008) 014016, arXiv:0712.2670.

[42] J. Bartels, K. J. Golec-Biernat, and H. Kowalski, *A modification of the saturation model: DGLAP evolution*, Phys. Rev. D **66** (2002) 014001, arXiv:hep-ph/0203258.

[43] W. Buchmuller and S. H. H. Tye, *Quarkonia and quantum chromodynamics*, Phys. Rev. **D24** (1981) 132.

[44] A. Martin, *A fit of upsilon and charmonium spectra*, Phys. Lett. **B93** (1980) 338.

[45] N. Barik and S. N. Jena, *Fine-hyperfine splittings of quarkonium levels in an effective power-law potential*, Phys. Lett. **B97** (1980) 265.

[46] K. J. Golec-Biernat and M. Wusthoff, *Saturation effects in deep inelastic scattering at low $Q^2$ and its implications on diffraction*, Phys. Rev. **D59** (1998) 014017, arXiv:hep-ph/9807513.

[47] K. J. Golec-Biernat and M. Wusthoff, *Saturation in diffractive deep inelastic scattering*, Phys. Rev. **D60** (1999) 114023, arXiv:hep-ph/9903358.

[48] B. Z. Kopeliovich, A. Schafer, and A. V. Tarasov, *Nonperturbative effects in gluon radiation and photoproduction of quark pairs*, Phys. Rev. **D62** (2000) 054022, arXiv:hep-ph/9908245.

[49] V. N. Gribov, *Glauber corrections and the interaction between high-energy hadrons and nuclei*, Sov. Phys. JETP **29** (1969) 483.

[50] J. Hufner, B. Kopeliovich, and J. Nemchik, *Glauber multiple scattering theory for the photoproduction of vector mesons off nuclei and the role of the coherence length*, Phys. Lett. **B383** (1996) 362, arXiv:nucl-th/9605007.

[51] B. Z. Kopeliovich, *Gribov inelastic shadowing in the dipole representation*, Int. J. Mod. Phys. **A31** (2016) 1645021, arXiv:1602.00298.

# LHCb collaboration

R. Aaij[32], A.S.W. Abdelmotteleb[50], C. Abellan Beteta[44], F. Abudinén[50], T. Ackernley[54], B. Adeva[40], M. Adinolfi[48], H. Afsharnia[9], C. Agapopoulou[13], C.A. Aidala[76], S. Aiola[25], Z. Ajaltouni[9], S. Akar[59], K. Akiba[32], J. Albrecht[15], F. Alessio[42], M. Alexander[53], A. Alfonso Albero[39], Z. Aliouche[56], P. Alvarez Cartelle[49], R. Amalric[13], S. Amato[2], J.L. Amey[48], Y. Amhis[11,42], L. An[42], L. Anderlini[22], M. Andersson[44], A. Andreianov[38], M. Andreotti[21], D. Andreou[62], D. Ao[6], F. Archilli[17], A. Artamonov[38], M. Artuso[62], E. Aslanides[10], M. Atzeni[44], B. Audurier[12], S. Bachmann[17], M. Bachmayer[43], J.J. Back[50], A. Bailly-reyre[13], P. Baladron Rodriguez[40], V. Balagura[12], W. Baldini[21], J. Baptista de Souza Leite[1], M. Barbetti[22,j], R.J. Barlow[56], S. Barsuk[11], W. Barter[55], M. Bartolini[49], F. Baryshnikov[38], J.M. Basels[14], G. Bassi[29,q], B. Batsukh[4], A. Battig[15], A. Bay[43], A. Beck[50], M. Becker[15], F. Bedeschi[29], I.B. Bediaga[1], A. Beiter[62], V. Belavin[38], S. Belin[40], V. Bellee[44], K. Belous[38], I. Belov[38], I. Belyaev[38], G. Benane[10], G. Bencivenni[23], E. Ben-Haim[13], A. Berezhnoy[38], R. Bernet[44], D. Berninghoff[17], H.C. Bernstein[62], C. Bertella[56], A. Bertolin[28], C. Betancourt[44], F. Betti[42], Ia. Bezshyiko[44], S. Bhasin[48], J. Bhom[35], L. Bian[67], M.S. Bieker[15], N.V. Biesuz[21], S. Bifani[47], P. Billoir[13], A. Biolchini[32], M. Birch[55], F.C.R. Bishop[49], A. Bitadze[56], A. Bizzeti, M.P. Blago[49], T. Blake[50], F. Blanc[43], S. Blusk[62], D. Bobulska[53], J.A. Boelhauve[15], O. Boente Garcia[12], T. Boettcher[59], A. Boldyrev[38], C.S. Bolognani[73], N. Bondar[38,42], S. Borghi[56], M. Borsato[17], J.T. Borsuk[35], S.A. Bouchiba[43], T.J.V. Bowcock[54,42], A. Boyer[42], C. Bozzi[21], M.J. Bradley[55], S. Braun[60], A. Brea Rodriguez[40], J. Brodzicka[35], A. Brossa Gonzalo[50], D. Brundu[27], A. Buonaura[44], L. Buonincontri[28], A.T. Burke[56], C. Burr[42], A. Bursche[66], A. Butkevich[38], J.S. Butter[32], J. Buytaert[42], W. Byczynski[42], S. Cadeddu[27], H. Cai[67], R. Calabrese[21,i], L. Calefice[15,13], S. Cali[23], R. Calladine[47], M. Calvi[26,m], M. Calvo Gomez[74], P. Camargo Magalhaes[48], P. Campana[23], D.H. Campora Perez[73], A.F. Campoverde Quezada[6], S. Capelli[26,m], L. Capriotti[20,g], A. Carbone[20,g], G. Carboni[31], R. Cardinale[24,k], A. Cardini[27], I. Carli[4], P. Carniti[26,m], L. Carus[14], A. Casais Vidal[40], R. Caspary[17], G. Casse[54], M. Cattaneo[42], G. Cavallero[42], V. Cavallini[21,i], S. Celani[43], J. Cerasoli[10], D. Cervenkov[57], A.J. Chadwick[54], M.G. Chapman[48], M. Charles[13], Ph. Charpentier[42], C.A. Chavez Barajas[54], M. Chefdeville[8], C. Chen[3], S. Chen[4], A. Chernov[35], S. Chernyshenko[46], V. Chobanova[40], S. Cholak[43], M. Chrzaszcz[35], A. Chubykin[38], V. Chulikov[38], P. Ciambrone[23], M.F. Cicala[50], X. Cid Vidal[40], G. Ciezarek[42], G. Ciullo[i,21], P.E.L. Clarke[52], M. Clemencic[42], H.V. Cliff[49], J. Closier[42], J.L. Cobbledick[56], V. Coco[42], J.A.B. Coelho[11], J. Cogan[10], E. Cogneras[9], L. Cojocariu[37], P. Collins[42], T. Colombo[42], L. Congedo[19], A. Contu[27], N. Cooke[47], G. Coombs[53], I. Corredoira [40], G. Corti[42], B. Couturier[42], D.C. Craik[58], J. Crkovská[61], M. Cruz Torres[1,e], R. Currie[52], C.L. Da Silva[61], S. Dadabaev[38], L. Dai[65], X. Dai[5], E. Dall'Occo[15], J. Dalseno[40], C. D'Ambrosio[42], A. Danilina[38], P. d'Argent[15], J.E. Davies[56], A. Davis[56], O. De Aguiar Francisco[56], J. de Boer[42], K. De Bruyn[72], S. De Capua[56], M. De Cian[43], U. De Freitas Carneiro Da Graca[1], E. De Lucia[23], J.M. De Miranda[1], L. De Paula[2], M. De Serio[19,f], D. De Simone[44], P. De Simone[23], F. De Vellis[15], J.A. de Vries[73], C.T. Dean[61], F. Debernardis[19,f], D. Decamp[8], V. Dedu[10], L. Del Buono[13], B. Delaney[58], H.-P. Dembinski[15], V. Denysenko[44], O. Deschamps[9], F. Dettori[27,h], B. Dey[70], A. Di Cicco[23], P. Di Nezza[23], I. Diachkov[38],

S. Didenko[38], L. Dieste Maronas[40], S. Ding[62], V. Dobishuk[46], A. Dolmatov[38], C. Dong[3], A.M. Donohoe[18], F. Dordei[27], A.C. dos Reis[1], L. Douglas[53], A.G. Downes[8], W. Duan[66], M.W. Dudek[35], L. Dufour[42], V. Duk[71], P. Durante[42], J.M. Durham[61], D. Dutta[56], A. Dziurda[35], A. Dzyuba[38], S. Easo[51], U. Egede[63], V. Egorychev[38], S. Eidelman[38,†], C. Eirea Orro[40], S. Eisenhardt[52], S. Ek-In[43], L. Eklund[75], S. Ely[62], A. Ene[37], E. Epple[61], S. Escher[14], J. Eschle[44], S. Esen[44], T. Evans[56], L.N. Falcao[1], Y. Fan[6], B. Fang[67], S. Farry[54], D. Fazzini[26,m], M. Feo[42], A.D. Fernez[60], F. Ferrari[20], L. Ferreira Lopes[43], F. Ferreira Rodrigues[2], S. Ferreres Sole[32], M. Ferrillo[44], M. Ferro-Luzzi[42], S. Filippov[38], R.A. Fini[19], M. Fiorini[21,i], M. Firlej[34], K.M. Fischer[57], D.S. Fitzgerald[76], C. Fitzpatrick[56], T. Fiutowski[34], F. Fleuret[12], M. Fontana[13], F. Fontanelli[24,k], R. Forty[42], D. Foulds-Holt[49], V. Franco Lima[54], M. Franco Sevilla[60], M. Frank[42], E. Franzoso[21,i], G. Frau[17], C. Frei[42], D.A. Friday[53], J. Fu[6], Q. Fuehring[15], E. Gabriel[32], G. Galati[19,f], M.D. Galati[72], A. Gallas Torreira[40], D. Galli[20,g], S. Gambetta[52,42], Y. Gan[3], M. Gandelman[2], P. Gandini[25], Y. Gao[5], M. Garau[27,h], L.M. Garcia Martin[50], P. Garcia Moreno[39], J. García Pardiñas[26,m], B. Garcia Plana[40], F.A. Garcia Rosales[12], L. Garrido[39], C. Gaspar[42], R.E. Geertsema[32], D. Gerick[17], L.L. Gerken[15], E. Gersabeck[56], M. Gersabeck[56], T. Gershon[50], L. Giambastiani[28], V. Gibson[49], H.K. Giemza[36], A.L. Gilman[57], M. Giovannetti[23,t], A. Gioventù[40], P. Gironella Gironell[39], C. Giugliano[21,i], M.A. Giza[35], K. Gizdov[52], E.L. Gkougkousis[42], V.V. Gligorov[13,42], C. Göbel[64], E. Golobardes[74], D. Golubkov[38], A. Golutvin[55,38], A. Gomes[1,a], S. Gomez Fernandez[39], F. Goncalves Abrantes[57], M. Goncerz[35], G. Gong[3], I.V. Gorelov[38], C. Gotti[26], J.P. Grabowski[17], T. Grammatico[13], L.A. Granado Cardoso[42], E. Graugés[39], E. Graverini[43], G. Graziani, A. T. Grecu[37], L.M. Greeven[32], N.A. Grieser[4], L. Grillo[53], S. Gromov[38], B.R. Gruberg Cazon[57], C. Gu[3], M. Guarise[21,i], M. Guittiere[11], P. A. Günther[17], E. Gushchin[38], A. Guth[14], Y. Guz[38], T. Gys[42], T. Hadavizadeh[63], G. Haefeli[43], C. Haen[42], J. Haimberger[42], S.C. Haines[49], T. Halewood-leagas[54], M.M. Halvorsen[42], P.M. Hamilton[60], J. Hammerich[54], Q. Han[7], X. Han[17], E.B. Hansen[56], S. Hansmann-Menzemer[17,42], L. Hao[6], N. Harnew[57], T. Harrison[54], C. Hasse[42], M. Hatch[42], J. He[6,c], K. Heijhoff[32], K. Heinicke[15], C. Henderson[59], R.D.L. Henderson[63,50], A.M. Hennequin[58], K. Hennessy[54], L. Henry[42], J. Heuel[14], A. Hicheur[2], D. Hill[43], M. Hilton[56], S.E. Hollitt[15], R. Hou[7], Y. Hou[8], J. Hu[17], J. Hu[66], W. Hu[5], X. Hu[3], W. Huang[6], X. Huang[67], W. Hulsbergen[32], R.J. Hunter[50], M. Hushchyn[38], D. Hutchcroft[54], P. Ibis[15], M. Idzik[34], D. Ilin[38], P. Ilten[59], A. Inglessi[38], A. Iniukhin[38], A. Ishteev[38], K. Ivshin[38], R. Jacobsson[42], H. Jage[14], S.J. Jaimes Elles[41], S. Jakobsen[42], E. Jans[32], B.K. Jashal[41], A. Jawahery[60], V. Jevtic[15], X. Jiang[4,6], Y. Jiang[6], M. John[57], D. Johnson[58], C.R. Jones[49], T.P. Jones[50], B. Jost[42], N. Jurik[42], I. Juszczak[35], S. Kandybei[45], Y. Kang[3], M. Karacson[42], D. Karpenkov[38], M. Karpov[38], J.W. Kautz[59], F. Keizer[42], D.M. Keller[62], M. Kenzie[50], T. Ketel[33], B. Khanji[15], A. Kharisova[38], S. Kholodenko[38], T. Kirn[14], V.S. Kirsebom[43], O. Kitouni[58], S. Klaver[33], N. Kleijne[29,q], K. Klimaszewski[36], M.R. Kmiec[36], S. Koliiev[46], A. Kondybayeva[38], A. Konoplyannikov[38], P. Kopciewicz[34], R. Kopecna[17], P. Koppenburg[32], M. Korolev[38], I. Kostiuk[32,46], O. Kot[46], S. Kotriakhova, A. Kozachuk[38], P. Kravchenko[38], L. Kravchuk[38], R.D. Krawczyk[42], M. Kreps[50], S. Kretzschmar[14], P. Krokovny[38], W. Krupa[34], W. Krzemien[36], J. Kubat[17], W. Kucewicz[35,34], M. Kucharczyk[35], V. Kudryavtsev[38], G.J. Kunde[61], A. Kupsc[75], D. Lacarrere[42], G. Lafferty[56], A. Lai[27], A. Lampis[27,h], D. Lancierini[44], C. Landesa Gomez[40],

J.J. Lane[56], R. Lane[48], G. Lanfranchi[23], C. Langenbruch[14], J. Langer[15], O. Lantwin[38], T. Latham[50], F. Lazzari[29,u], M. Lazzaroni[25,l], R. Le Gac[10], S.H. Lee[76], R. Lefèvre[9], A. Leflat[38], S. Legotin[38], P. Lenisa[i,21], O. Leroy[10], T. Lesiak[35], B. Leverington[17], A. Li[3], H. Li[66], K. Li[7], P. Li[17], S. Li[7], T. Li[66], Y. Li[4], Z. Li[62], X. Liang[62], C. Lin[6], T. Lin[51], R. Lindner[42], V. Lisovskyi[15], R. Litvinov[27,h], G. Liu[66], H. Liu[6], Q. Liu[6], S. Liu[4,6], A. Lobo Salvia[39], A. Loi[27], R. Lollini[71], J. Lomba Castro[40], I. Longstaff[53], J.H. Lopes[2], S. López Soliño[40], G.H. Lovell[49], Q. Lu[66], Y. Lu[4,b], C. Lucarelli[22,j], D. Lucchesi[28,o], S. Luchuk[38], M. Lucio Martinez[32], V. Lukashenko[32,46], Y. Luo[3], A. Lupato[56], E. Luppi[21,i], A. Lusiani[29,q], K. Lynch[18], X.-R. Lyu[6], L. Ma[4], R. Ma[6], S. Maccolini[20], F. Machefert[11], F. Maciuc[37], V. Macko[43], P. Mackowiak[15], S. Maddrell-Mander[48], L.R. Madhan Mohan[48], A. Maevskiy[38], D. Maisuzenko[38], M.W. Majewski[34], J.J. Malczewski[35], S. Malde[57], B. Malecki[35,42], A. Malinin[38], T. Maltsev[38], H. Malygina[17], G. Manca[27,h], G. Mancinelli[10], D. Manuzzi[20], C.A. Manzari[44], D. Marangotto[25,l], J.F. Marchand[8], U. Marconi[20], S. Mariani[22,j], C. Marin Benito[39], M. Marinangeli[43], J. Marks[17], A.M. Marshall[48], P.J. Marshall[54], G. Martelli[71,p], G. Martellotti[30], L. Martinazzoli[42,m], M. Martinelli[26,m], D. Martinez Santos[40], F. Martinez Vidal[41], A. Massafferri[1], M. Materok[14], R. Matev[42], A. Mathad[44], V. Matiunin[38], C. Matteuzzi[26], K.R. Mattioli[76], A. Mauri[32], E. Maurice[12], J. Mauricio[39], M. Mazurek[42], M. McCann[55], L. Mcconnell[18], T.H. McGrath[56], N.T. McHugh[53], A. McNab[56], R. McNulty[18], J.V. Mead[54], B. Meadows[59], G. Meier[15], D. Melnychuk[36], S. Meloni[26,m], M. Merk[32,73], A. Merli[25,l], L. Meyer Garcia[2], D. Miao[4,6], M. Mikhasenko[69,d], D.A. Milanes[68], E. Millard[50], M. Milovanovic[42], M.-N. Minard[8,†], A. Minotti[26,m], S.E. Mitchell[52], B. Mitreska[56], D.S. Mitzel[15], A. Mödden [15], R.A. Mohammed[57], R.D. Moise[55], S. Mokhnenko[38], T. Mombächer[40], I.A. Monroy[68], S. Monteil[9], M. Morandin[28], G. Morello[23], M.J. Morello[29,q], J. Moron[34], A.B. Morris[69], A.G. Morris[50], R. Mountain[62], H. Mu[3], F. Muheim[52], M. Mulder[72], K. Müller[44], C.H. Murphy[57], D. Murray[56], R. Murta[55], P. Muzzetto[27,h], P. Naik[48], T. Nakada[43], R. Nandakumar[51], T. Nanut[42], I. Nasteva[2], M. Needham[52], N. Neri[25,l], S. Neubert[69], N. Neufeld[42], P. Neustroev[38], R. Newcombe[55], E.M. Niel[43], S. Nieswand[14], N. Nikitin[38], N.S. Nolte[58], C. Normand[8,h,27], J. Novoa Fernandez[40], C. Nunez[76], A. Oblakowska-Mucha[34], V. Obraztsov[38], T. Oeser[14], D.P. O'Hanlon[48], S. Okamura[21,i], R. Oldeman[27,h], F. Oliva[52], M.E. Olivares[62], C.J.G. Onderwater[72], R.H. O'Neil[52], J.M. Otalora Goicochea[2], T. Ovsiannikova[38], P. Owen[44], A. Oyanguren[41], O. Ozcelik[52], K.O. Padeken[69], B. Pagare[50], P.R. Pais[42], T. Pajero[57], A. Palano[19], M. Palutan[23], Y. Pan[56], G. Panshin[38], A. Papanestis[51], M. Pappagallo[19,f], L.L. Pappalardo[21,i], C. Pappenheimer[59], W. Parker[60], C. Parkes[56], B. Passalacqua[21,i], G. Passaleva[22], A. Pastore[19], M. Patel[55], C. Patrignani[20,g], C.J. Pawley[73], A. Pearce[42], A. Pellegrino[32], M. Pepe Altarelli[42], S. Perazzini[20], D. Pereima[38], A. Pereiro Castro[40], P. Perret[9], M. Petric[53], K. Petridis[48], A. Petrolini[24,k], A. Petrov[38], S. Petrucci[52], M. Petruzzo[25], H. Pham[62], A. Philippov[38], R. Piandani[6], L. Pica[29,q], M. Piccini[71], B. Pietrzyk[8], G. Pietrzyk[11], M. Pili[57], D. Pinci[30], F. Pisani[42], M. Pizzichemi[26,m,42], V. Placinta[37], J. Plews[47], M. Plo Casasus[40], F. Polci[13,42], M. Poli Lener[23], M. Poliakova[62], A. Poluektov[10], N. Polukhina[38], I. Polyakov[42], E. Polycarpo[2], S. Ponce[42], D. Popov[6,42], S. Popov[38], S. Poslavskii[38], K. Prasanth[35], L. Promberger[42], C. Prouve[40], V. Pugatch[46], V. Puill[11], G. Punzi[29,r], H.R. Qi[3], W. Qian[6], N. Qin[3], S. Qu[3], R. Quagliani[43], N.V. Raab[18], R.I. Rabadan Trejo[6],

B. Rachwal[34], J.H. Rademacker[48], R. Rajagopalan[62], M. Rama[29], M. Ramos Pernas[50], M.S. Rangel[2], F. Ratnikov[38], G. Raven[33,42], M. Rebollo De Miguel[41], F. Redi[42], F. Reiss[56], C. Remon Alepuz[41], Z. Ren[3], V. Renaudin[57], P.K. Resmi[10], R. Ribatti[29,q], A.M. Ricci[27], S. Ricciardi[51], M. Richardson-Slipper[52], K. Rinnert[54], P. Robbe[11], G. Robertson[52], A.B. Rodrigues[43], E. Rodrigues[54], J.A. Rodriguez Lopez[68], E. Rodriguez Rodriguez[40], A. Rollings[57], P. Roloff[42], V. Romanovskiy[38], M. Romero Lamas[40], A. Romero Vidal[40], J.D. Roth[76,†], M. Rotondo[23], M.S. Rudolph[62], T. Ruf[42], R.A. Ruiz Fernandez[40], J. Ruiz Vidal[41], A. Ryzhikov[38], J. Ryzka[34], J.J. Saborido Silva[40], N. Sagidova[38], N. Sahoo[47], B. Saitta[27,h], M. Salomoni[42], C. Sanchez Gras[32], I. Sanderswood[41], R. Santacesaria[30], C. Santamarina Rios[40], M. Santimaria[23], E. Santovetti[31,t], D. Saranin[38], G. Sarpis[14], M. Sarpis[69], A. Sarti[30], C. Satriano[30,s], A. Satta[31], M. Saur[15], D. Savrina[38], H. Sazak[9], L.G. Scantlebury Smead[57], A. Scarabotto[13], S. Schael[14], S. Scherl[54], M. Schiller[53], H. Schindler[42], M. Schmelling[16], B. Schmidt[42], S. Schmitt[14], O. Schneider[43], A. Schopper[42], M. Schubiger[32], S. Schulte[43], M.H. Schune[11], R. Schwemmer[42], B. Sciascia[23,42], A. Sciuccati[42], S. Sellam[40], A. Semennikov[38], M. Senghi Soares[33], A. Sergi[24,k], N. Serra[44], L. Sestini[28], A. Seuthe[15], Y. Shang[5], D.M. Shangase[76], M. Shapkin[38], I. Shchemerov[38], L. Shchutska[43], T. Shears[54], L. Shekhtman[38], Z. Shen[5], S. Sheng[4,6], V. Shevchenko[38], B. Shi[6], E.B. Shields[26,m], Y. Shimizu[11], E. Shmanin[38], J.D. Shupperd[62], B.G. Siddi[21,i], R. Silva Coutinho[44], G. Simi[28], S. Simone[19,f], M. Singla[63], N. Skidmore[56], R. Skuza[17], T. Skwarnicki[62], M.W. Slater[47], J.C. Smallwood[57], J.G. Smeaton[49], E. Smith[44], K. Smith[61], M. Smith[55], A. Snoch[32], L. Soares Lavra[9], M.D. Sokoloff[59], F.J.P. Soler[53], A. Solomin[38,48], A. Solovev[38], I. Solovyev[38], F.L. Souza De Almeida[2], B. Souza De Paula[2], B. Spaan[15,†], E. Spadaro Norella[25,l], E. Spiridenkov[38], P. Spradlin[53], V. Sriskaran[42], F. Stagni[42], M. Stahl[59], S. Stahl[42], S. Stanislaus[57], E.N. Stein[42], O. Steinkamp[44], O. Stenyakin[38], H. Stevens[15], S. Stone[62,†], D. Strekalina[38], F. Suljik[57], J. Sun[27], L. Sun[67], Y. Sun[60], P. Svihra[56], P.N. Swallow[47], K. Swientek[34], A. Szabelski[36], T. Szumlak[34], M. Szymanski[42], Y. Tan[3], S. Taneja[56], A.R. Tanner[48], M.D. Tat[57], A. Terentev[38], F. Teubert[42], E. Thomas[42], D.J.D. Thompson[47], K.A. Thomson[54], H. Tilquin[55], V. Tisserand[9], S. T'Jampens[8], M. Tobin[4], L. Tomassetti[21,i], G. Tonani[25,l], X. Tong[5], D. Torres Machado[1], D.Y. Tou[3], E. Trifonova[38], S.M. Trilov[48], C. Trippl[43], G. Tuci[6], A. Tully[43], N. Tuning[32,42], A. Ukleja[36], D.J. Unverzagt[17], E. Ursov[38], A. Usachov[32], A. Ustyuzhanin[38], U. Uwer[17], A. Vagner[38], V. Vagnoni[20], A. Valassi[42], G. Valenti[20], N. Valls Canudas[74], M. van Beuzekom[32], M. Van Dijk[43], H. Van Hecke[61], E. van Herwijnen[38], M. van Veghel[72], R. Vazquez Gomez[39], P. Vazquez Regueiro[40], C. Vázquez Sierra[42], S. Vecchi[21], J.J. Velthuis[48], M. Veltri[22,v], A. Venkateswaran[62], M. Veronesi[32], M. Vesterinen[50], D. Vieira[59], M. Vieites Diaz[43], X. Vilasis-Cardona[74], E. Vilella Figueras[54], A. Villa[20], P. Vincent[13], F.C. Volle[11], D. vom Bruch[10], A. Vorobyev[38], V. Vorobyev[38], N. Voropaev[38], K. Vos[73], C. Vrahas[52], R. Waldi[17], J. Walsh[29], G. Wan[5], C. Wang[17], J. Wang[5], J. Wang[4], J. Wang[3], J. Wang[67], M. Wang[5], R. Wang[48], X. Wang[66], Y. Wang[7], Z. Wang[44], Z. Wang[3], Z. Wang[6], J.A. Ward[50,63], N.K. Watson[47], D. Websdale[55], Y. Wei[5], C. Weisser[58], B.D.C. Westhenry[48], D.J. White[56], M. Whitehead[53], A.R. Wiederhold[50], D. Wiedner[15], G. Wilkinson[57], M.K. Wilkinson[59], I. Williams[49], M. Williams[58], M.R.J. Williams[52], R. Williams[49], F.F. Wilson[51], W. Wislicki[36], M. Witek[35], L. Witola[17], C.P. Wong[61], G. Wormser[11], S.A. Wotton[49], H. Wu[62], K. Wyllie[42], Z. Xiang[6], D. Xiao[7],

Y. Xie[7], A. Xu[5], J. Xu[6], L. Xu[3], L. Xu[3], M. Xu[50], Q. Xu[6], Z. Xu[9], Z. Xu[6], D. Yang[3], S. Yang[6], Y. Yang[6], Z. Yang[5], Z. Yang[60], L.E. Yeomans[54], H. Yin[7], J. Yu[65], X. Yuan[62], E. Zaffaroni[43], M. Zavertyaev[16], M. Zdybal[35], O. Zenaiev[42], M. Zeng[3], C. Zhang[5], D. Zhang[7], L. Zhang[3], S. Zhang[65], S. Zhang[5], Y. Zhang[5], Y. Zhang[57], A. Zharkova[38], A. Zhelezov[17], Y. Zheng[6], T. Zhou[5], X. Zhou[6], Y. Zhou[6], V. Zhovkovska[11], X. Zhu[3], X. Zhu[7], Z. Zhu[6], V. Zhukov[14,38], Q. Zou[4,6], S. Zucchelli[20,g], D. Zuliani[28], G. Zunica[56].

[1] *Centro Brasileiro de Pesquisas Físicas (CBPF), Rio de Janeiro, Brazil*
[2] *Universidade Federal do Rio de Janeiro (UFRJ), Rio de Janeiro, Brazil*
[3] *Center for High Energy Physics, Tsinghua University, Beijing, China*
[4] *Institute Of High Energy Physics (IHEP), Beijing, China*
[5] *School of Physics State Key Laboratory of Nuclear Physics and Technology, Peking University, Beijing, China*
[6] *University of Chinese Academy of Sciences, Beijing, China*
[7] *Institute of Particle Physics, Central China Normal University, Wuhan, Hubei, China*
[8] *Université Savoie Mont Blanc, CNRS, IN2P3-LAPP, Annecy, France*
[9] *Université Clermont Auvergne, CNRS/IN2P3, LPC, Clermont-Ferrand, France*
[10] *Aix Marseille Univ, CNRS/IN2P3, CPPM, Marseille, France*
[11] *Université Paris-Saclay, CNRS/IN2P3, IJCLab, Orsay, France*
[12] *Laboratoire Leprince-Ringuet, CNRS/IN2P3, Ecole Polytechnique, Institut Polytechnique de Paris, Palaiseau, France*
[13] *LPNHE, Sorbonne Université, Paris Diderot Sorbonne Paris Cité, CNRS/IN2P3, Paris, France*
[14] *I. Physikalisches Institut, RWTH Aachen University, Aachen, Germany*
[15] *Fakultät Physik, Technische Universität Dortmund, Dortmund, Germany*
[16] *Max-Planck-Institut für Kernphysik (MPIK), Heidelberg, Germany*
[17] *Physikalisches Institut, Ruprecht-Karls-Universität Heidelberg, Heidelberg, Germany*
[18] *School of Physics, University College Dublin, Dublin, Ireland*
[19] *INFN Sezione di Bari, Bari, Italy*
[20] *INFN Sezione di Bologna, Bologna, Italy*
[21] *INFN Sezione di Ferrara, Ferrara, Italy*
[22] *INFN Sezione di Firenze, Firenze, Italy*
[23] *INFN Laboratori Nazionali di Frascati, Frascati, Italy*
[24] *INFN Sezione di Genova, Genova, Italy*
[25] *INFN Sezione di Milano, Milano, Italy*
[26] *INFN Sezione di Milano-Bicocca, Milano, Italy*
[27] *INFN Sezione di Cagliari, Monserrato, Italy*
[28] *Università degli Studi di Padova, Università e INFN, Padova, Padova, Italy*
[29] *INFN Sezione di Pisa, Pisa, Italy*
[30] *INFN Sezione di Roma La Sapienza, Roma, Italy*
[31] *INFN Sezione di Roma Tor Vergata, Roma, Italy*
[32] *Nikhef National Institute for Subatomic Physics, Amsterdam, Netherlands*
[33] *Nikhef National Institute for Subatomic Physics and VU University Amsterdam, Amsterdam, Netherlands*
[34] *AGH - University of Science and Technology, Faculty of Physics and Applied Computer Science, Kraków, Poland*
[35] *Henryk Niewodniczanski Institute of Nuclear Physics Polish Academy of Sciences, Kraków, Poland*
[36] *National Center for Nuclear Research (NCBJ), Warsaw, Poland*
[37] *Horia Hulubei National Institute of Physics and Nuclear Engineering, Bucharest-Magurele, Romania*
[38] *Affiliated with an institute covered by a cooperation agreement with CERN*
[39] *ICCUB, Universitat de Barcelona, Barcelona, Spain*
[40] *Instituto Galego de Física de Altas Enerxías (IGFAE), Universidade de Santiago de Compostela, Santiago de Compostela, Spain*
[41] *Instituto de Fisica Corpuscular, Centro Mixto Universidad de Valencia - CSIC, Valencia, Spain*
[42] *European Organization for Nuclear Research (CERN), Geneva, Switzerland*
[43] *Institute of Physics, Ecole Polytechnique Fédérale de Lausanne (EPFL), Lausanne, Switzerland*

[44] *Physik-Institut, Universität Zürich, Zürich, Switzerland*
[45] *NSC Kharkiv Institute of Physics and Technology (NSC KIPT), Kharkiv, Ukraine*
[46] *Institute for Nuclear Research of the National Academy of Sciences (KINR), Kyiv, Ukraine*
[47] *University of Birmingham, Birmingham, United Kingdom*
[48] *H.H. Wills Physics Laboratory, University of Bristol, Bristol, United Kingdom*
[49] *Cavendish Laboratory, University of Cambridge, Cambridge, United Kingdom*
[50] *Department of Physics, University of Warwick, Coventry, United Kingdom*
[51] *STFC Rutherford Appleton Laboratory, Didcot, United Kingdom*
[52] *School of Physics and Astronomy, University of Edinburgh, Edinburgh, United Kingdom*
[53] *School of Physics and Astronomy, University of Glasgow, Glasgow, United Kingdom*
[54] *Oliver Lodge Laboratory, University of Liverpool, Liverpool, United Kingdom*
[55] *Imperial College London, London, United Kingdom*
[56] *Department of Physics and Astronomy, University of Manchester, Manchester, United Kingdom*
[57] *Department of Physics, University of Oxford, Oxford, United Kingdom*
[58] *Massachusetts Institute of Technology, Cambridge, MA, United States*
[59] *University of Cincinnati, Cincinnati, OH, United States*
[60] *University of Maryland, College Park, MD, United States*
[61] *Los Alamos National Laboratory (LANL), Los Alamos, NM, United States*
[62] *Syracuse University, Syracuse, NY, United States*
[63] *School of Physics and Astronomy, Monash University, Melbourne, Australia, associated to* [50]
[64] *Pontifícia Universidade Católica do Rio de Janeiro (PUC-Rio), Rio de Janeiro, Brazil, associated to* [2]
[65] *Physics and Micro Electronic College, Hunan University, Changsha City, China, associated to* [7]
[66] *Guangdong Provincial Key Laboratory of Nuclear Science, Guangdong-Hong Kong Joint Laboratory of Quantum Matter, Institute of Quantum Matter, South China Normal University, Guangzhou, China, associated to* [3]
[67] *School of Physics and Technology, Wuhan University, Wuhan, China, associated to* [3]
[68] *Departamento de Fisica , Universidad Nacional de Colombia, Bogota, Colombia, associated to* [13]
[69] *Universität Bonn - Helmholtz-Institut für Strahlen und Kernphysik, Bonn, Germany, associated to* [17]
[70] *Eotvos Lorand University, Budapest, Hungary, associated to* [42]
[71] *INFN Sezione di Perugia, Perugia, Italy, associated to* [21]
[72] *Van Swinderen Institute, University of Groningen, Groningen, Netherlands, associated to* [32]
[73] *Universiteit Maastricht, Maastricht, Netherlands, associated to* [32]
[74] *DS4DS, La Salle, Universitat Ramon Llull, Barcelona, Spain, associated to* [39]
[75] *Department of Physics and Astronomy, Uppsala University, Uppsala, Sweden, associated to* [53]
[76] *University of Michigan, Ann Arbor, MI, United States, associated to* [62]

[a] *Universidade Federal do Triângulo Mineiro (UFTM), Uberaba-MG, Brazil*
[b] *Central South U., Changsha, China*
[c] *Hangzhou Institute for Advanced Study, UCAS, Hangzhou, China*
[d] *Excellence Cluster ORIGINS, Munich, Germany*
[e] *Universidad Nacional Autónoma de Honduras, Tegucigalpa, Honduras*
[f] *Università di Bari, Bari, Italy*
[g] *Università di Bologna, Bologna, Italy*
[h] *Università di Cagliari, Cagliari, Italy*
[i] *Università di Ferrara, Ferrara, Italy*
[j] *Università di Firenze, Firenze, Italy*
[k] *Università di Genova, Genova, Italy*
[l] *Università degli Studi di Milano, Milano, Italy*
[m] *Università di Milano Bicocca, Milano, Italy*
[n] *Università di Modena e Reggio Emilia, Modena, Italy*
[o] *Università di Padova, Padova, Italy*
[p] *Università di Perugia, Perugia, Italy*
[q] *Scuola Normale Superiore, Pisa, Italy*
[r] *Università di Pisa, Pisa, Italy*
[s] *Università della Basilicata, Potenza, Italy*
[t] *Università di Roma Tor Vergata, Roma, Italy*
[u] *Università di Siena, Siena, Italy*

[v] *Università di Urbino, Urbino, Italy*

[†] *Deceased*